Work Summary

Advancing the tight-binding model by using double cavities. Derived the ground state of Hubbard model of half-filled 4 sites tight-binding model.

Main Work

1. Derivations for Hubbard model ground state under 4 sites
2. Additional details on double cavity control
3. Code analysis
4. Simulation results for dynamics

1 Derivations for Hubbard model ground state under 4 sites

Following the conventions set in Prof. Girvin's book, let the hopping magnitude be t instead of J in the previous reports. In Hubbard model,

$$\hat{H} = \hat{T} + \hat{V},$$

where

$$\hat{T} = -t \sum_{i,\sigma} \left(\hat{c}^{\dagger}_{i,\sigma} \hat{c}_{i+1,\sigma} + \hat{c}^{\dagger}_{i+1,\sigma} \hat{c}_{i,\sigma} \right)$$

and

$$\hat{V} = U \sum_{i} \hat{n}_{i,\uparrow} \hat{n}_{i,\downarrow}.$$

In the case of U/t $\gg$ 1, the ground state can be solved with perturbation theory. It is desirable to find an effective Hamiltonian for the low energy states, i.e. no double occupation. Divide the hopping Hamiltonian into

$$\hat{T} = \hat{T}_0 + \hat{T}_+ + \hat{T}_-$$

such that $\hat{T}_0$ conserves the number of double occupation states, and $\hat{T}_\pm$ increase/decrease the number of double occupation states by one. Here, construct an unitary such that in the rotating frame, the effective Hamiltonian do not have first order $\hat{T}_\pm$, which can lead low energy states to high energy states. Construct the unitary to be $\hat{W} = e^{\hat{S}}$, where $\hat{S} = \lambda(\hat{T}_+ - \hat{T}_-)$. The effective Hamiltonian is then

$$\hat{H}' = \hat{W}\hat{H}\hat{W}^{\dagger} = \hat{H} + \left[\hat{S}, \hat{H}\right] + \frac{1}{2!}\left[\hat{S}\left[\hat{S}, \hat{H}\right]\right] + \cdots .$$

Considering the definitions of $\hat{T}_{0,\pm 1}$, it is straightforward that $\left[\hat{V}, \hat{T}_m\right] = mU\hat{T}_m$, where m takes values 0 and ± 1. Then,

$$\begin{aligned}
\hat{H}' &= \hat{W}\hat{H}\hat{W}^\dagger \\
&= \hat{H} + \left[\hat{S}, \hat{H}\right] + \frac{1}{2!}\left[\hat{S}\left[\hat{S}, \hat{H}\right]\right] + \cdots \\
&= \hat{V} + \hat{T}_0 + \left(\hat{T}_+ + \hat{T}_-\right) + \lambda\left(\left[\hat{T}_+, \hat{V}\right] - \left[\hat{T}_-, \hat{V}\right] + \left[\hat{T}_+ - \hat{T}_-, \hat{T}\right]\right) + \frac{1}{2}\left[\hat{S}\left[\hat{S}, \hat{V}\right]\right] + \mathcal{O}(\lambda^2 t^3) \\
&= \hat{V} + \hat{T}_0 + (1-\lambda U)\left(\hat{T}_+ + \hat{T}_-\right) + \lambda\left(\left[\hat{T}_+ - \hat{T}_-, \hat{T}\right]\right) - \frac{\lambda^2 U}{2}\left[\hat{T}_+ - \hat{T}_-, \hat{T}_+ + \hat{T}_-\right]\mathcal{O}(\lambda^2 t^3) \\
&= \hat{V} + \hat{T}_0 + (1-\lambda U)\left(\hat{T}_+ + \hat{T}_-\right) + \lambda\left(\left[\hat{T}_+ - \hat{T}_-, \hat{T}\right]\right) - \lambda^2 U\left[\hat{T}_+, \hat{T}_-\right] + \mathcal{O}(\lambda^2 t^3). \qquad (1)
\end{aligned}$$

Therefore, to get rid of the term linear in $\hat{T}_\pm$, let $\lambda = 1/U$. Note that

$$\left[\hat{T}_+ - \hat{T}_-, \hat{T}\right] = \left[\hat{T}_+, \hat{T}_-\right] + \left[\hat{T}_+, \hat{T}_0\right] - \left[\hat{T}_-, \hat{T}_0\right] - \left[\hat{T}_-, \hat{T}_+\right] = 2\left[\hat{T}_+, \hat{T}_-\right] + \left[\hat{T}_+, \hat{T}_0\right] - \left[\hat{T}_-, \hat{T}_0\right].$$

When in the low energy states, there are no doubly occupied states, therefore $\hat{T}_-$ and $\hat{V}$ always returns 0. If considering half-filled, then $\hat{T}_0$ also gives 0. Since $\hat{T}_0 = \hat{T}_0^\dagger$, the term $\hat{T}_0\hat{T}_+$ also vanishes. Thus

$$\hat{H}' = -\frac{1}{U}\hat{T}_-\hat{T}_+.$$

For 4 sites, the state are represented by the braket notation and if any site is double occupied, it is noted such as $|-, \uparrow\downarrow, \uparrow, \uparrow\rangle$. The commas separate out the 4 sites. Without special notation, there is no double occupied sites. Also, let the state annihilation operators be defined to act with an ordering from 1 to 4. For example, $|\uparrow\uparrow\downarrow\downarrow\rangle = \hat{c}^\dagger_{1,\uparrow}\hat{c}^\dagger_{2,\uparrow}\hat{c}^\dagger_{3,\downarrow}\hat{c}^\dagger_{4,\downarrow}|0\rangle$. The double occupied states should first apply spin up operator then spin down operator.

The possible low energy states can be divided different 'kinds' by the number of spin up and spin down electrons they have. The effective Hamiltonian will have zero matrix elements across the different kinds. For example, one kind is when there are two spin up and two spin down electrons. Possible ones are $|\uparrow\uparrow\downarrow\downarrow\rangle$, $|\downarrow\uparrow\uparrow\downarrow\rangle$, $|\downarrow\downarrow\uparrow\uparrow\rangle$, $|\uparrow\downarrow\downarrow\uparrow\rangle$, $|\downarrow\uparrow\downarrow\uparrow\rangle$, and $|\uparrow\downarrow\uparrow\downarrow\rangle$, where the last two are the *Néel* states. Some sample calculations are as follows,

$$\begin{aligned}
\frac{\hat{T}_+}{-t}|\uparrow\uparrow\downarrow\downarrow\rangle &= \left(\hat{c}^\dagger_{4,\uparrow}\hat{c}_{1,\uparrow} + \hat{c}^\dagger_{3,\uparrow}\hat{c}_{2,\uparrow} + \hat{c}^\dagger_{1,\downarrow}\hat{c}_{4,\downarrow} + \hat{c}^\dagger_{2,\downarrow}\hat{c}_{3,\downarrow}\right)\hat{c}^\dagger_{1,\uparrow}\hat{c}^\dagger_{2,\uparrow}\hat{c}_{3,\downarrow}\hat{c}_{4,\downarrow}|0\rangle \\
&= |-, \uparrow, \downarrow, \uparrow\downarrow\rangle + |\uparrow, -, \uparrow\downarrow, \downarrow\rangle + |\uparrow\downarrow, \uparrow, \downarrow, -\rangle + |\uparrow, \uparrow\downarrow, -, \downarrow\rangle \\
\frac{\hat{T}_+}{-t}|\downarrow\uparrow\uparrow\downarrow\rangle &= -|-, \uparrow\downarrow, \uparrow, \downarrow\rangle - |\uparrow\downarrow, -, \uparrow, \downarrow\rangle + |\downarrow, \uparrow, -, \uparrow\downarrow\rangle + |\downarrow, \uparrow, \uparrow\downarrow, -\rangle \\
\frac{\hat{T}_+}{-t}|\downarrow\downarrow\uparrow\uparrow\rangle &= -|-, \downarrow, \uparrow, \uparrow\downarrow\rangle - |\downarrow, -, \uparrow\downarrow, \uparrow\rangle - |\downarrow, \uparrow\downarrow, -, \uparrow\rangle - |\uparrow\downarrow, \downarrow, \uparrow, -\rangle \\
\frac{\hat{T}_+}{-t}|\uparrow\downarrow\downarrow\uparrow\rangle &= |-, \uparrow\downarrow, \downarrow, \uparrow\rangle + |\uparrow\downarrow, -, \downarrow, \uparrow\rangle - |\uparrow, \downarrow, -, \uparrow\downarrow\rangle - |\uparrow, \downarrow, \uparrow\downarrow, -\rangle \\
\frac{\hat{T}_+}{-t}|\uparrow\downarrow\uparrow\downarrow\rangle &= |-, \uparrow\downarrow, \uparrow, \downarrow\rangle + |-, \downarrow, \uparrow, \uparrow\downarrow\rangle + |\uparrow\downarrow, -, \uparrow, \downarrow\rangle - |\uparrow, -, \uparrow\downarrow, \downarrow\rangle \\
&\quad -|\uparrow, \uparrow\downarrow, -, \downarrow\rangle + |\uparrow, \downarrow, -, \uparrow\downarrow\rangle + |\uparrow, \downarrow, \uparrow\downarrow, -\rangle + |\uparrow\downarrow, \downarrow, \uparrow, -\rangle \\
\frac{\hat{T}_+}{-t}|\downarrow\uparrow\downarrow\uparrow\rangle &= -|-, \uparrow\downarrow, \downarrow, \uparrow\rangle - |-, \uparrow, \downarrow, \uparrow\downarrow\rangle - |\uparrow\downarrow, -, \downarrow, \uparrow\rangle + |\downarrow, -, \uparrow\downarrow, \uparrow\rangle \\
&\quad +|\downarrow, \uparrow\downarrow, -, \uparrow\rangle - |\downarrow, \uparrow\ -, \uparrow\downarrow\rangle - |\downarrow, \uparrow, \uparrow\downarrow, -\rangle - |\uparrow\downarrow, \uparrow, \downarrow, -\rangle \qquad (2)
\end{aligned}$$

Expressing in the basis of $\begin{pmatrix} |\uparrow\uparrow\downarrow\downarrow\rangle \\ |\downarrow\uparrow\uparrow\downarrow\rangle \\ |\downarrow\downarrow\uparrow\uparrow\rangle \\ |\uparrow\downarrow\downarrow\uparrow\rangle \\ |\uparrow\downarrow\uparrow\downarrow\rangle \\ |\downarrow\uparrow\downarrow\uparrow\rangle \end{pmatrix}$, the effective Hamiltonian is then $-\frac{t^2}{U}\begin{pmatrix} 4 & 0 & 0 & 0 & -2 & -2 \\ 0 & 4 & 0 & 0 & -2 & -2 \\ 0 & 0 & 4 & 0 & -2 & -2 \\ 0 & 0 & 0 & 4 & -2 & -2 \\ -2 & -2 & -2 & -2 & 4 & 0 \\ -2 & -2 & -2 & -2 & 0 & 4 \end{pmatrix}$.
Finding the lowest eigenvalue of this matrix gives the ground state energy $E_{ground} = -4\left(1+\sqrt{2}\right)\frac{t^2}{U}$.

The corresponding ground state is $\frac{1}{2}\begin{pmatrix} \frac{1}{\sqrt{2}} \\ \frac{1}{\sqrt{2}} \\ \frac{1}{\sqrt{2}} \\ \frac{1}{\sqrt{2}} \\ -1 \\ -1 \end{pmatrix}$. The energy of the *Néel* states are $\langle\downarrow\uparrow\downarrow\uparrow|\hat{H}'|\downarrow\uparrow\downarrow\uparrow\rangle = -\frac{4t^2}{U}$, which is $\frac{4\sqrt{2}t^2}{U}$ above the ground state.

2 Additional details on double cavity control

Following from the formulations in the previous report, the controls can be expressed as

$$\left\{\hat{a}_1+\hat{a}_1^\dagger, i\left(\hat{a}_1-\hat{a}_1^\dagger\right), \sigma_{1,x}, \sigma_{1,y}\right\} \text{ and } \left\{\hat{a}_2+\hat{a}_2^\dagger, i\left(\hat{a}_2-\hat{a}_2^\dagger\right), \sigma_{2,x}, \sigma_{2,y}\right\}$$

acting separately on the two cavity-qubit systems. In order to have the two cavities talk to each other, there is also the controls from the beam splitter that takes photon from one cavity to another

$$\left\{\hat{a}_1^\dagger\hat{a}_2+\hat{a}_1\hat{a}_2^\dagger, i\left(\hat{a}_1^\dagger\hat{a}_2-\hat{a}_1\hat{a}_2^\dagger\right)\right\}$$

or the controls from the mode squeezer

$$\left\{\hat{a}_1^\dagger\hat{a}_2^\dagger+\hat{a}_1\hat{a}_2, i\left(\hat{a}_1^\dagger\hat{a}_2^\dagger-\hat{a}_1\hat{a}_2\right)\right\}.$$

Note that only one of the beam splitter and mode squeezer can be applied (is this true?).

3 Code analysis

In Figure 1, it shows the profiling result for an example code run of GRAPE. It is clear from the graph that matrix multiplication, i.e. numpy.dot, has been taking the majority of the time (around 84.8%). This is mainly due to the number of matrix multiplications needed and the dimensions of the matrices. Worth noticing, there are a decent fraction of the matrix multiplications happening when calculating the fidelity gradients.

3.1 Attempts to optimize code

I have made the following attempts to optimize the run time of the code.

1. Parallelization. There are two parts that can be parallelly computed in general. I have tried both the built-in module of qutip, i.e. qutip.parallel.parallel_map, and qiskit's implementation,

Name	Call Count	Time (ms)	Own Time (ms)
<method 'dot' of 'numpy.ndarray' objects>	62375	305192 84.6%	305191 84.6%
eigh	840	22535 6.2%	22472 6.2%
_compute_prop_grad	8400	206258 57.2%	7721 2.1%
_combine_dyn_gen	840	6863 1.9%	6441 1.8%
_spectral_decomp	840	27199 7.5%	3942 1.1%
compute_fid_grad	21	129742 36.0%	1375 0.4%
<built-in method numpy.zeros>	10022	1313 0.4%	1313 0.4%
recompute_evolution	21	222663 61.7%	1273 0.4%
getmodule	773	2954 0.8%	1138 0.3%
<method 'read' of '_io.FileIO' objects>	774	956 0.3%	956 0.3%
<built-in method builtins.hasattr>	714988	683 0.2%	647 0.2%
<method 'trace' of 'numpy.ndarray' objects>	8422	483 0.1%	483 0.1%
_apply_phase_preop	850	436 0.1%	428 0.1%
<built-in method posix.stat>	7130	423 0.1%	423 0.1%
ismodule	704135	541 0.1%	351 0.1%
transform	8422	44224 12.3%	332 0.1%
<method 'conj' of 'numpy.ndarray' objects>	841	327 0.1%	327 0.1%
<built-in method builtins.isinstance>	817776	285 0.1%	277 0.1%

(a) Table

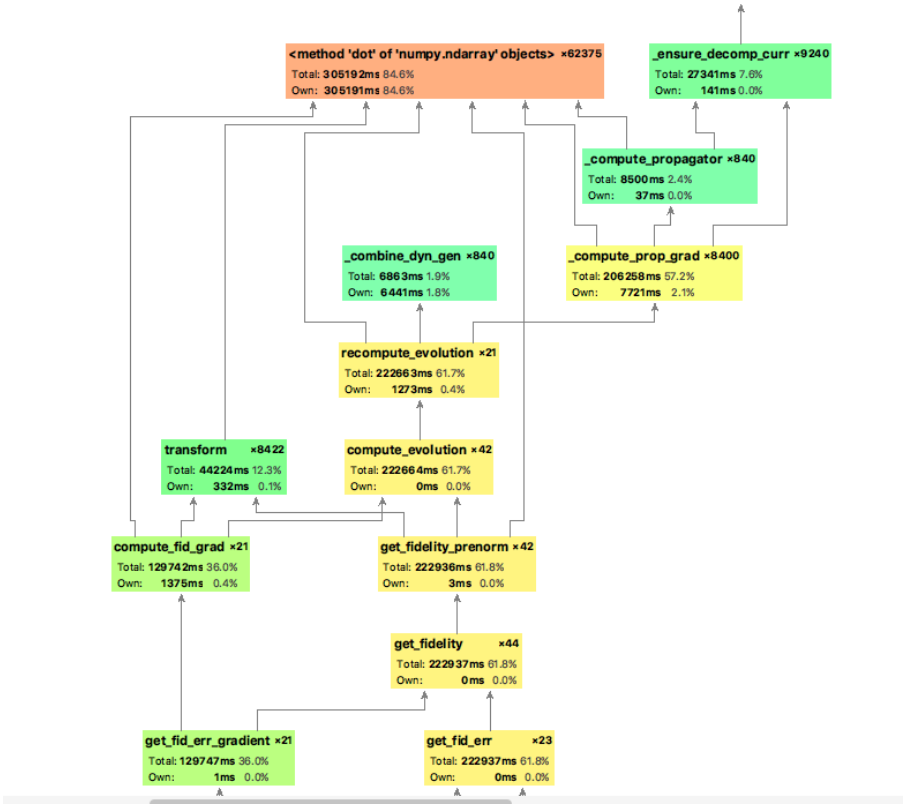

(b) Chart

Figure 1: Profiling result

both both failed, resulting in a even longer run time on the Princeton cluster. Both modules uses the library multiprocessing.

(a) When doing testing on parameters, the testings can be computed in parallel.

(b) The gradient calculations, as stated previously, are time consuming. The calculations of number $N_{ts} \times N_{ctrls}$ are independent, and therefore should be able to be computed in parllel.

2. Fidelity gradient calculation. The current method of QuTip is to simply run a for-loop over the $N_{ts} \times N_{ctrls}$ number of fidelity gradients needed. I modified the code to utilize numpy's matrix operation. Also, the fidelity gradients involves the calculation of matrix traces, and I have used its cyclic property to reduce the number of matrix multiplications needed. However, these only gives a not large speed-up by far.

3. Matrix data type. Currently, QuTip's implementation already takes advantages from CPython and sparse matrix. The matrices are in the data type of complex 128, meaning tracking the

complex entries with 64-bit float for each real and imaginary parts. I suspect that using complex 64 can have good-enough results and increase the speed. However, I tried but QuTip has implemented complex 128 very broadly, so it is very tedious to change all entries to complex 64.

4 Simulation results for dynamics

Now, the simulations are extended to more cases of single cavity and double cavities, and there can be either two spinless fermions or 1 spin up and 1 spin down electrons. Express the electron spin configurations as $[n_{up}, n_{down}]$ showing the number of spin up and down electrons. Therefore having 2 spinless fermions is equivalent as having electron spin configuration of [2, 0], and the second case is noted as [1,1].

4.1 Effect of number of time slices

Theoretically, having more number of time slices shouldn't harm the performance of GRAPE. However, practically speaking, having the least number of time slice while maintaining the performance on a decent level can greatly decrease the computational cost.

As shown in Figure 2, the trend of fidelity error vs the number of time slices are plotted for both cases of 2 spinless electrons and 1 spin up 1 spin down electron. Note here only single cavity is used. Worth noticing, as what's seen previously, using single cavity to simulate [1,1] does not yield satisfactory results. Even with 100 time slices and maximum iterations 2000, the infidelity is still just around 0.2. Therefore, the plot for [1,1] does not look at stable as [2,0] after increasing to certain number of time slices. However, it can still be spotted that for [2,0] and [1,1], the infidelity stabilized roughly after 30 and 60 number of time slices respectively.

This value of number of time slices required should be associated with the control power the system has. For [2,0] and [1,1] case, since only single cavity is used, each needs to access the first 6 and 16 energy levels. When using double cavities, however, there are more than double the number of controls, and it is roughly similar to accessing first 4 energy levels in single cavity. Thus, in the following, without special notice, I will use 40 time slices for simulating [2,0] in single cavity or [1,1] in double cavities, and use 80 time slices for simulating [1,1] in single cavity.

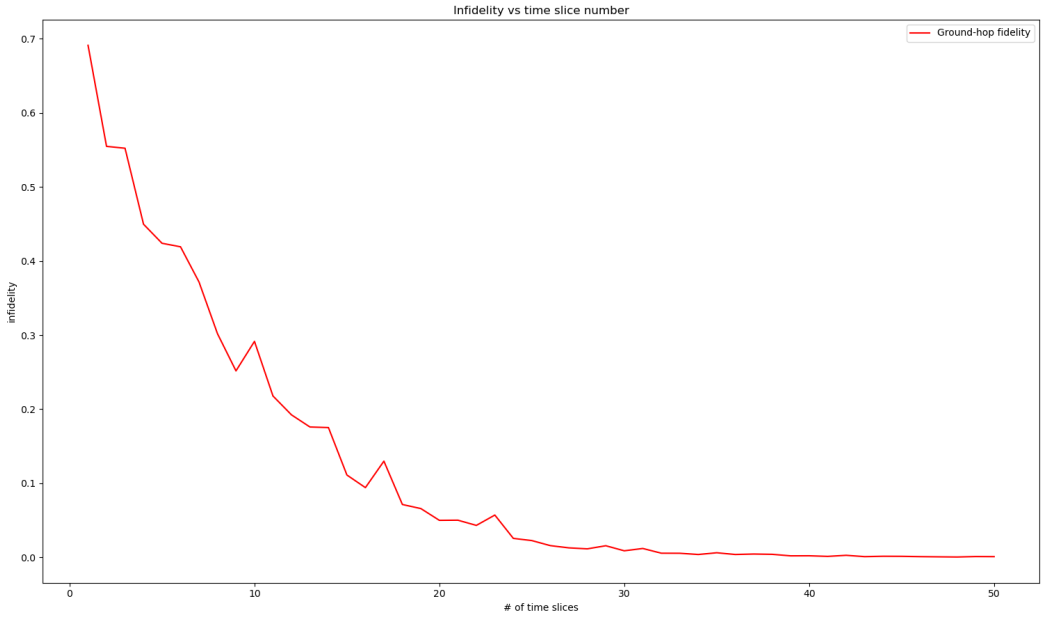

(a) Spins [2, 0], single cavity.

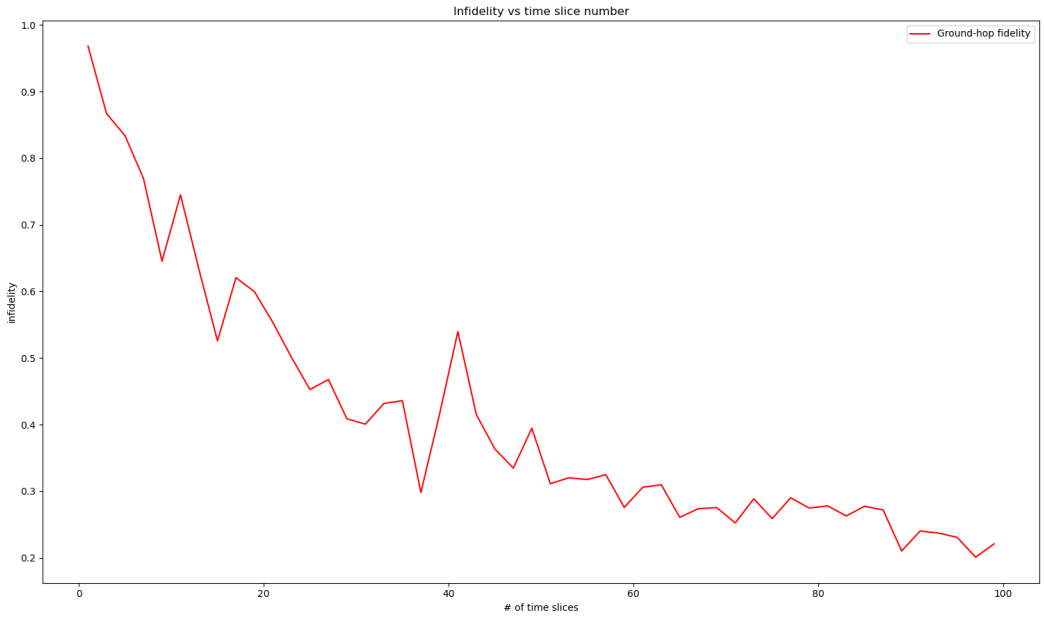

(b) Spins [1, 1], single cavity.

Figure 2: Infidelity vs number of time slices for both electron configurations. Maximum iteration set to be 2000 and evolution time 2.0μs.

4.2 Effect of the cavity Hilbert space truncation

Similar to what is noted in the previous section, the Hilbert space dimension should find an 'good enough' value such that the fidelity error stabilizes, i.e. when it tends to the actual value when driving in infinite dimensions.

As shown in Figure 3, the infidelity stabilizes roughly after 15 and 40 cavity energy levels for the case of [2,0] and [1,1] respectively. Therefore, later on, without specifications, the cavity energy levels used are 20 for [2,0] in single cavity, 40 for [1,1] in single cavity, and 10 for each cavity when simulating [1,1] in double cavities.

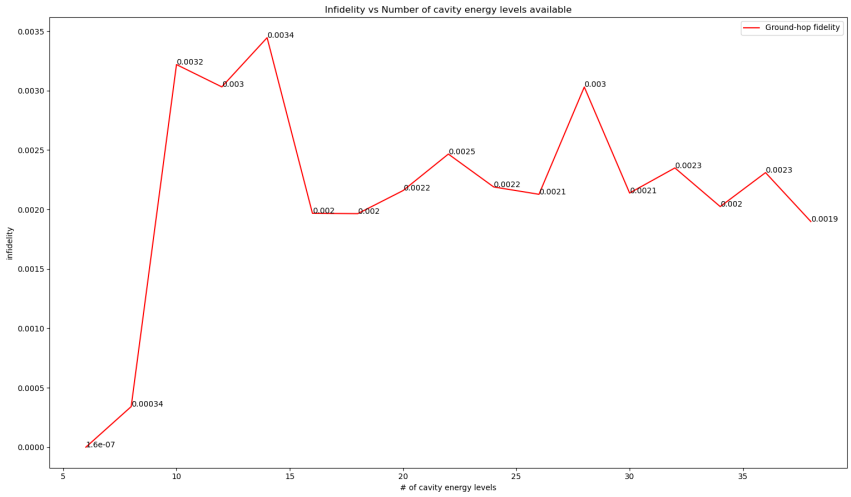

(a) Spins [2, 0], single cavity.

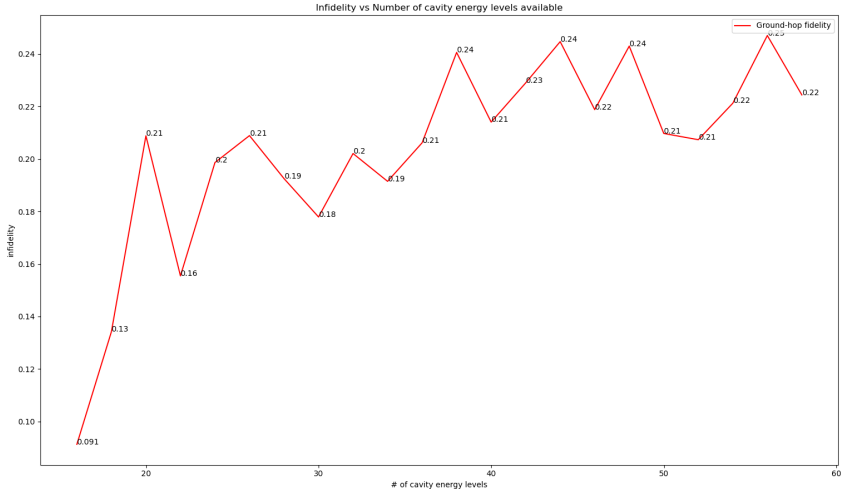

(b) Spins [1, 1], single cavity.

Figure 3: Infidelity vs truncated Hilbert space dimensions for both electron configurations. Maximum iteration set to be 2000 and evolution time 2.0μs.

The most time consuming part of the algorithm should be matrix multiplications, which has a complexity of $\mathcal{O}(n^{2.3737})$ for the fastest algorithm known. The computation time with respect to Hilbert space dimension is shown in Figure 4 for the case of simulating [2,0] in single cavity. The increase in

time is clearly polynomial from the plot. In the double cavity case, the increase can be even steeper since there are two cavities, so the Hilbert space dimension, i.e. the matrix dimension, increases with N_{cav}^2.

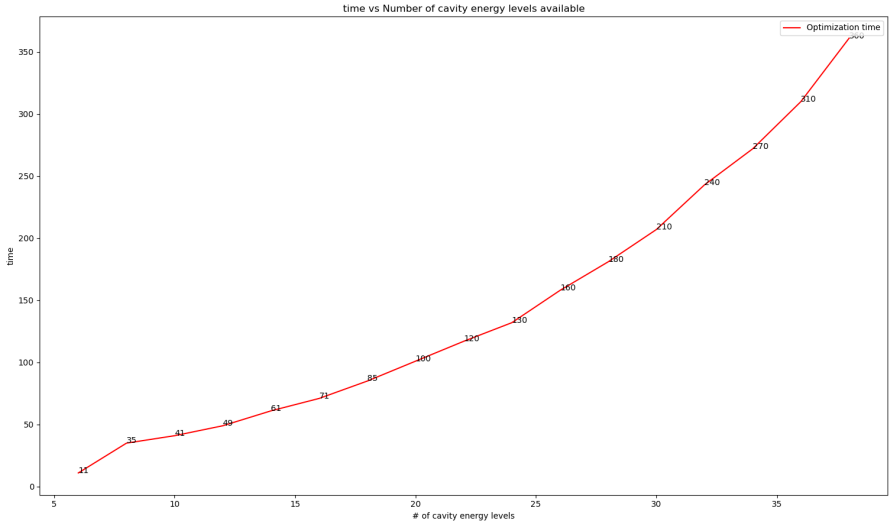

Figure 4: Algorithm run time vs truncated Hilbert space dimensions for [1,1] in single cavity.

To Do: another way of finding the optimum Hilbert space dimension can be to optimize the pulse sequence with N_{cav}, reaching a fidelity of f_{cav} comparing to the target unitary. Then, use the resulting pulse sequence to numerically drive the system in a safer, i.e. much larger, dimension N'_{cav} to obtain fidelity f'_{cav}. If f_{cav} and f'_{cav} are close enough, then N_{cav} is a good-to-use dimension.

4.3 Dynamics evolution for [1,1], double cavities

The dynamics evolution for [2,0] with single cavity has been shown in previous reports. Here, dynamics of [1,1] is shown. No satisfactory results have been obtained for single cavity, so here only presents ones using double cavities. The following sections uses either beam splitter controls or mode squeezer controls as described before.

For both cases, the system parameters are mostly set as usual. Some specifications are that the pulse sequence length is 2μs and 10 cavity energy levels are used for each cavity. There are two physical models explored. The simple model has no site Hamiltonian or nearest-neighbor interactions. While J being around 0.3 as usual, the full model has site Hamiltonian randomly chosen as [0.0976, 0.430, 0.206, 0.0898], and a nearest-neighbor interaction magnitude of $U/J = 0.1$.

Choose the initial state as $|c_1 q_1 c_2 q_2\rangle = \frac{1}{\sqrt{2}}\left(|0,0,0,0\rangle + |0,0,1,0\rangle\right)$. The Hamiltonian-driven evolution for both the simple model and the full model are shown in Figure 5. It is obvious that the symmetries are broken in the Full model with the random parameters selected.

On either simple or full mode, the pulse sequences with beam splitter control or mode squeezer control on double cavities are optimized, and their infidelity vs number of iterations are each shown in Figure 6. Note that all achieves around 10^{-3} infidelity at around 500 iterations, which is pretty impressive. However, running the 500 iterations takes around 4 hours already.

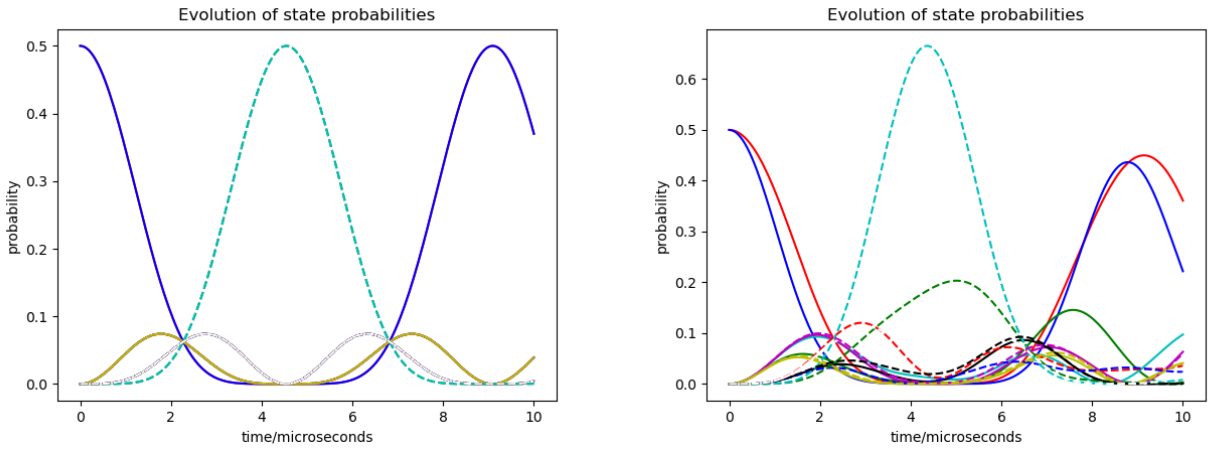

(a) Simple model (b) Full model

Figure 5: Hamiltonian-driven state evolution of the effective cavity energy level, i.e. the first 16 levels.

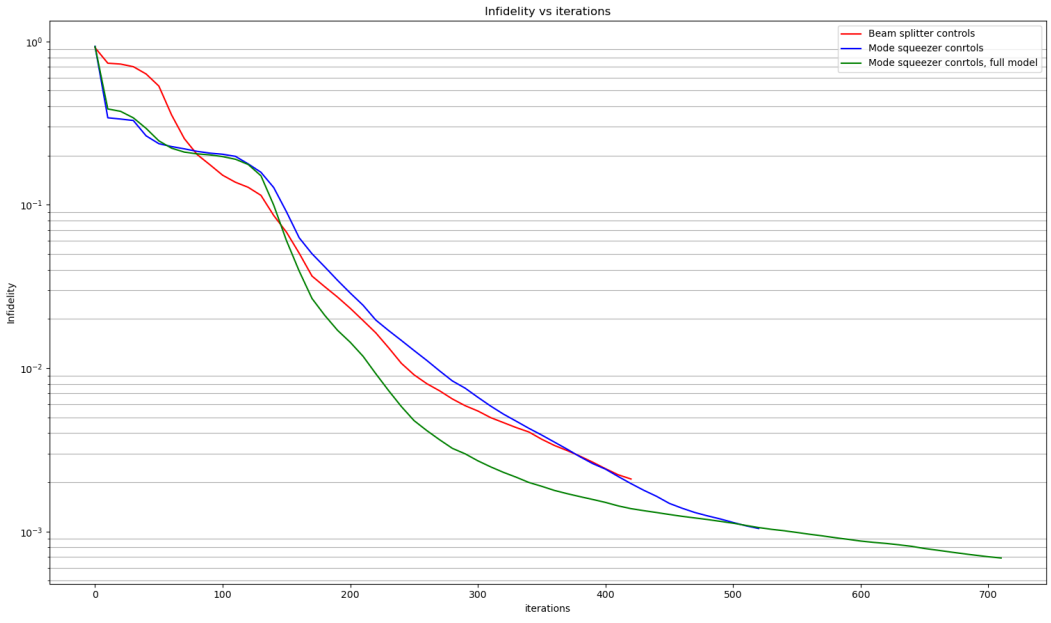

Figure 6: Infidelity vs number of iterations for [1,1] in double cavities with beam splitter or mode squeezer control. Assumes simple model if not labeled.

An example of the initial pulse sequence guess for the 10 controls for beam splitter is shown as in Figure 7. Note that because of the way the pulse guesses are made, these initial guess will be the same for the mode squeezer, just with the last two control replaced by the mode squeezer control at the same control amplitudes.

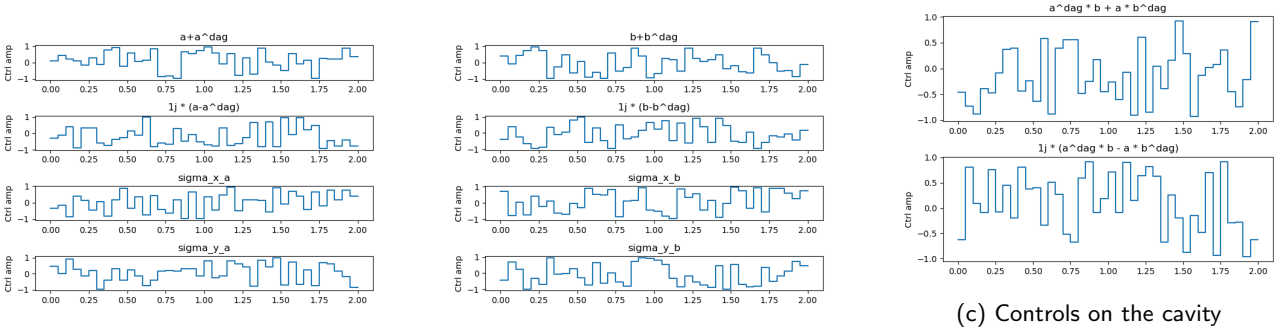

(a) Controls on the first cavity (b) Controls on the second cavity (c) Controls on the cavity interactions

Figure 7: Initial pulse sequences guess for double cavity with beam splitter controls.

4.3.1 Beam splitter, simple model

Figure 8 shows the final pulse sequences after optimization. Worth noticing that the controls on each cavities increases to a scale of around 10, but the control for the cavity interactions decreased in scale to around 0.1.

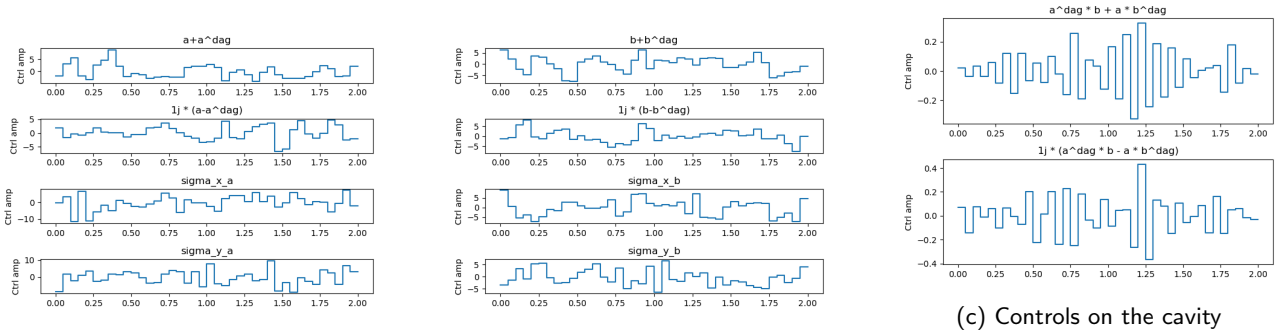

(a) Controls on the first cavity (b) Controls on the second cavity (c) Controls on the cavity interactions

Figure 8: Final pulse sequences for double cavity with beam splitter controls.

As an illustration of how the electron density looks like on each site, Figure 9 and 10 each shows the electron density evolution in 5 pulse sequences for the spin up and spin down electrons on the 4 sites.

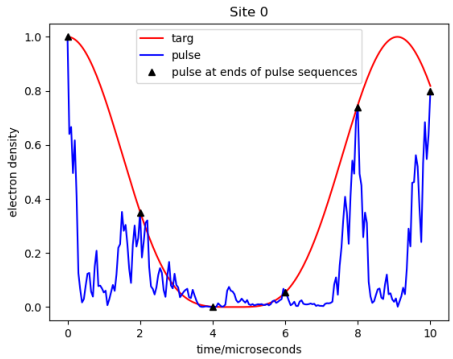

(a) Site 0

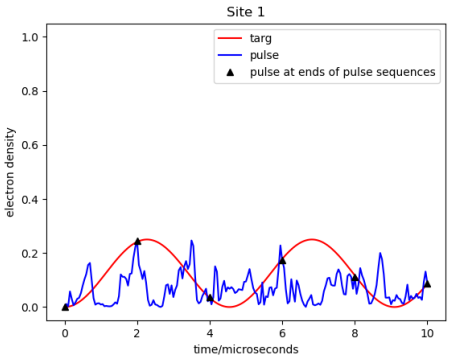

(b) Site 1

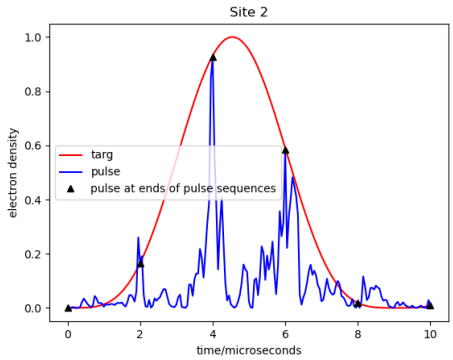

(c) Site 2

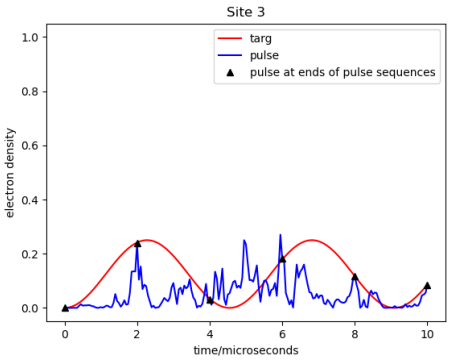

(d) Site 3

Figure 9: Spin up electron density evolution comparison between Hamiltonian-driven and pulse-driven dynamics.

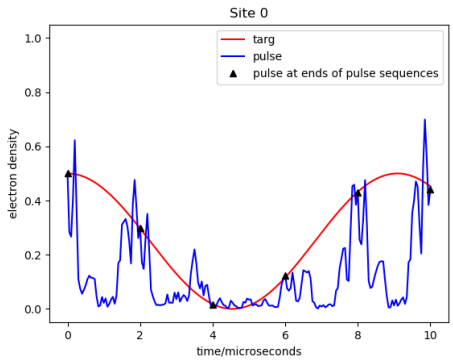

(a) Site 0

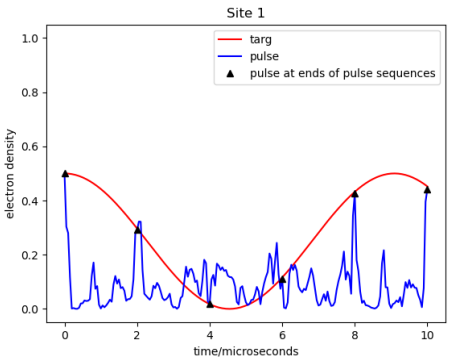

(b) Site 1

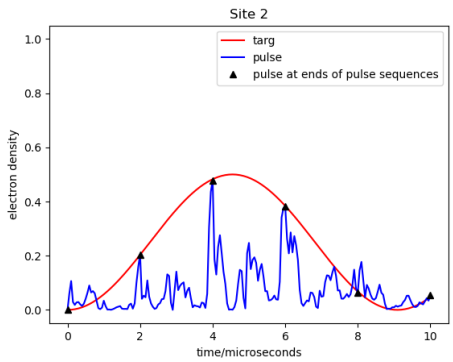

(c) Site 2

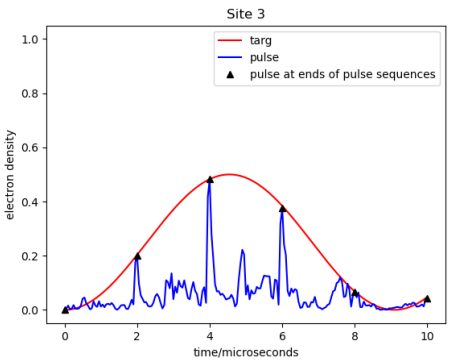

(d) Site 3

Figure 10: Spin down electron density evolution comparison between Hamiltonian-driven and pulse-driven dynamics.

To get an idea of how the electron density is leaked out of the effective energy levels (the first 16) in the pulse-driven dynamics, Figure 11 shows the electron leakage density, which is defined as the difference between the sum of electron densities on 4 sites and the theoretical sum. The theoretical sum is 1 for both spin up and down electrons in the case of [1,1].

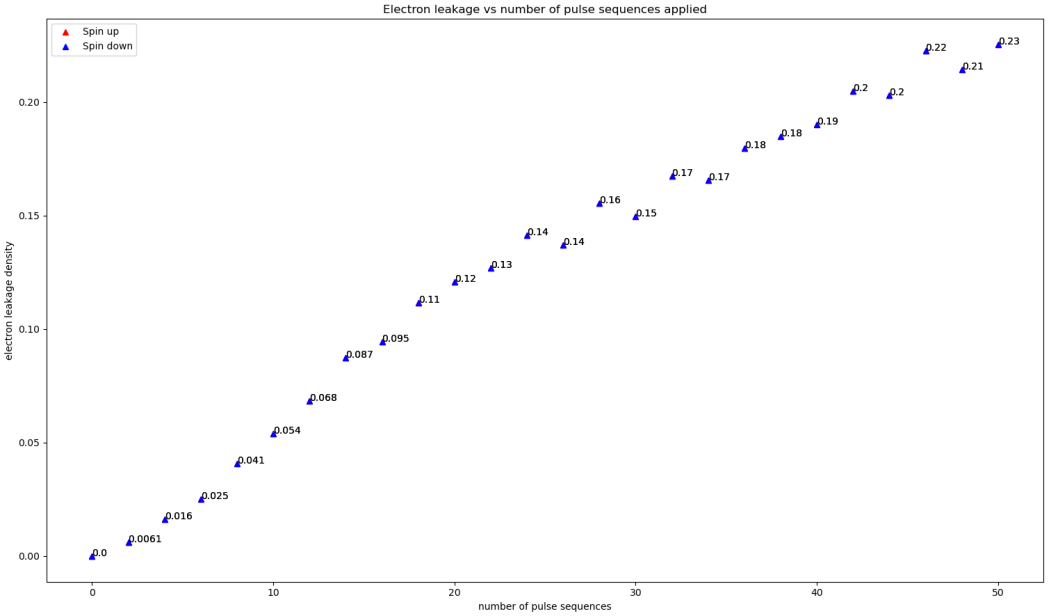

Figure 11: Electron density leaked outside of the effective energy levels vs the number of pulse sequences applied.

4.3.2 Mode squeezer, simple model

Figure 12 shows the final pulse sequences after optimization. Similarly, the control for the cavity interactions decreased in scale to around 0.1.

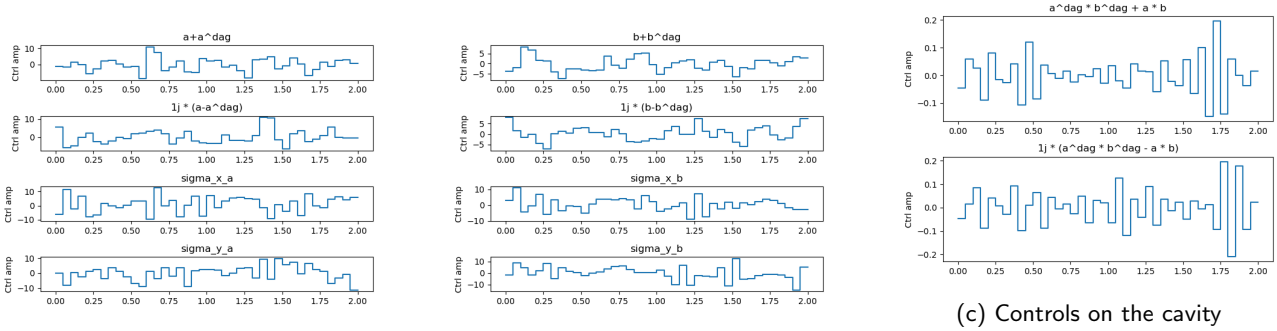

(a) Controls on the first cavity

(b) Controls on the second cavity

(c) Controls on the cavity interactions

Figure 12: Final pulse sequences for double cavity with mode squeezer controls.

As an illustration of how the electron density looks like on each site, Figure 13 and 14 each shows the electron density evolution in 5 pulse sequences for the spin up and spin down electrons on the 4 sites.

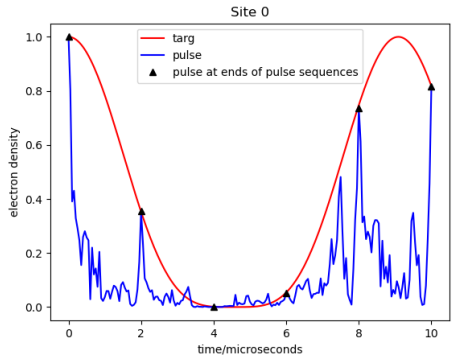

(a) Site 0

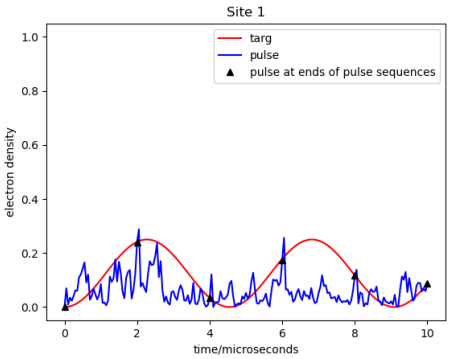

(b) Site 1

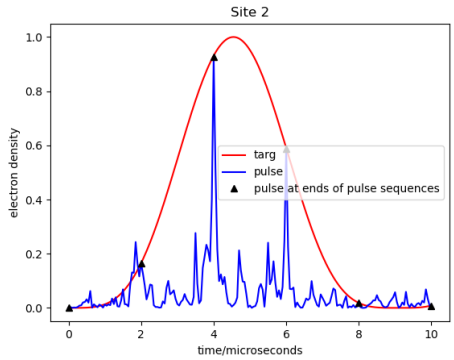

(c) Site 2

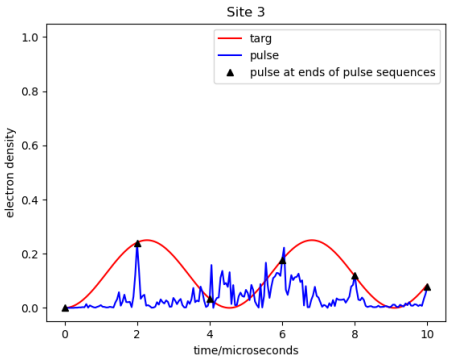

(d) Site 3

Figure 13: Spin up electron density evolution comparison between Hamiltonian-driven and pulse-driven dynamics.

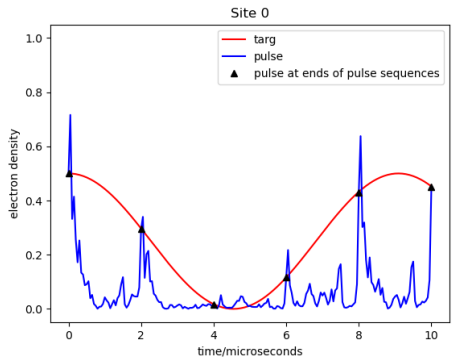

(a) Site 0

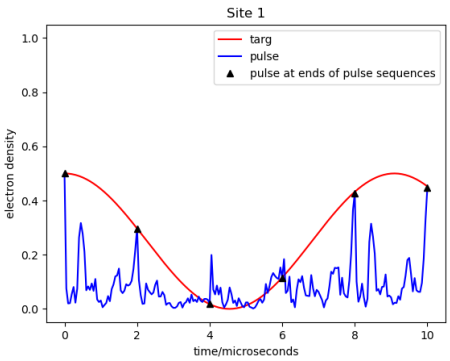

(b) Site 1

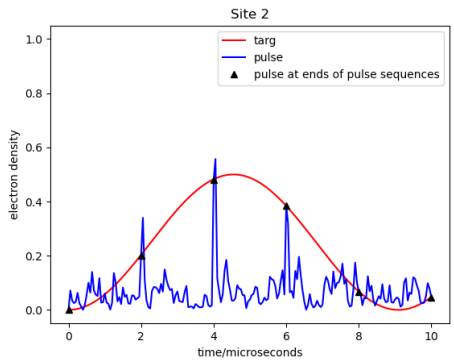

(c) Site 2

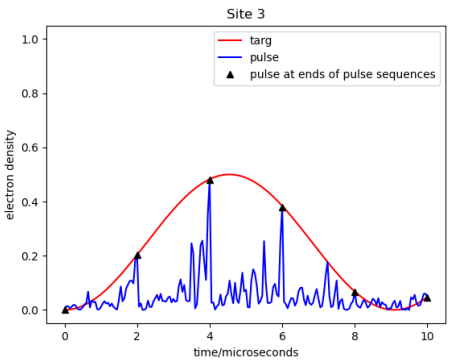

(d) Site 3

Figure 14: Spin down electron density evolution comparison between Hamiltonian-driven and pulse-driven dynamics.

Figure 15 shows the electron leakage density. Note that there is the unexpected peak and the electron density within the effective energy levels surprisingly starts to rise back. I think this might just be an exception given the result shown in the next section of mode squeezer acting on full model.

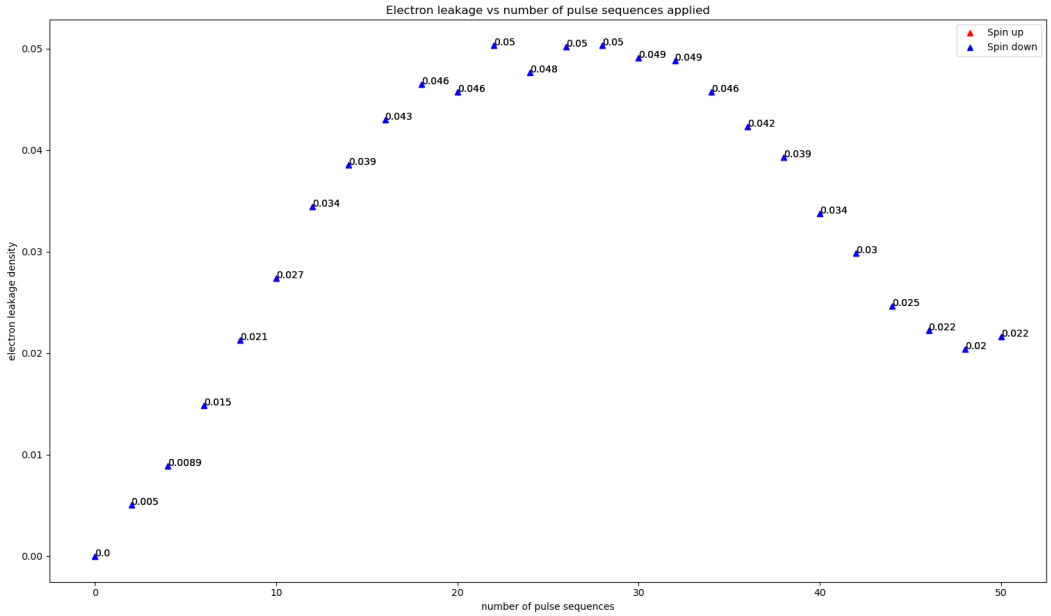

Figure 15: Electron density leaked outside of the effective energy levels vs the number of pulse sequences applied.

4.3.3 Mode squeezer, full model

For simplicity, the pulse sequences and comparisons of electron densities are not shown here. Figure 16 shows the electron leak density for the full model, which does not show the peak as shown in the previous section.

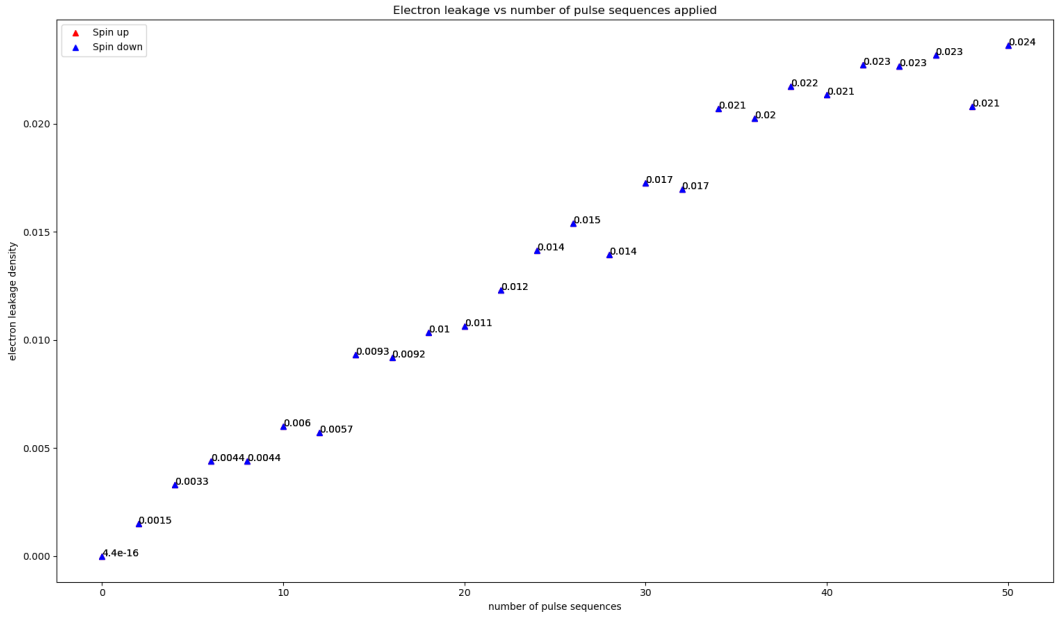

Figure 16: Electron density leaked outside of the effective energy levels vs the number of pulse sequences applied.